


Cite this: *RSC Adv.*, 2020, 10, 17359

Alkaline water-splitting reactions over Pd/Co-MOF-derived carbon obtained *via* microwave-assisted synthesis

Adewale K. Ipadeola  and Kenneth I. Ozoemena *

Cobalt-based metal–organic framework-derived carbon (MOFDC) has been studied as a new carbon-based support for a Pd catalyst for electrochemical water-splitting; *i.e.*, the hydrogen evolution reaction (HER) and oxygen evolution reaction (OER) in alkaline medium. The study shows a high increase in the HER activity, in terms of low onset overpotential (onset $\eta = 35$ mV vs. RHE), high exchange current density ($j_{0,s} \approx 0.22$ mA cm⁻²), high mass activity ($j_{0,m} \approx 59$ mA mg⁻¹), high kinetic current ($j_K \approx 5$ –8 mA cm⁻²) and heterogeneous rate constant ($k^0 \approx 4 \times 10^{-4}$ cm s⁻¹), which are attributed to the high porosity of MOFDC and contribution from residual Co, while the large Tafel slope ($b_c = 261$ mV dec⁻¹) is ascribed to the high degree of hydrogen adsorption onto polycrystalline Pd as a supplementary reaction step to the suggested Volmer–Heyrovsky mechanism. These values for the catalyst are comparable to or better than many recent reports that adopted nano-carbon materials and/or use bi- or ternary Pd-based electrocatalysts for the HER. The improved HER activity of Pd/MOFDC is associated with the positive impact of MOFDC and residual Co on the Pd catalyst (*i.e.*, low activation energy, $E_A \approx 12$ kJ mol⁻¹) which allows for easy desorption of the H_{ads} to generate hydrogen. Moreover, Pd/MOFDC displays better OER activity than its analogue, with lower onset η (1.29 V vs. RHE) and b_a (≈ 78 mV dec⁻¹), and higher current response (*ca.* 18 mA cm⁻²). Indeed, this study provides a new strategy of designing and synthesizing MOFDC with physico-chemical features for Pd-based electrocatalysts that will allow for efficient electrochemical water-splitting processes.

Received 11th March 2020

Accepted 24th April 2020

DOI: 10.1039/d0ra02307h

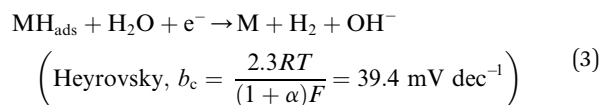
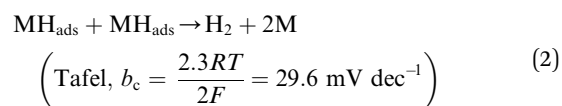
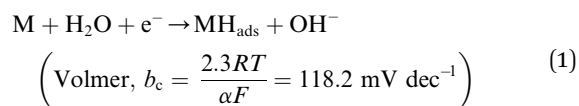
rsc.li/rsc-advances

1. Introduction

Hydrogen is an excellent fuel for the realization of clean and renewable energy. Hydrogen evolution reaction (HER) *via* electrochemical water-splitting process has become important in a world that strives for a clean environment and urgent mitigation of the negative consequences of climate change brought about by greenhouse gases. Efficient HER is generally dependent on the nature of electrocatalysts that drive the reaction.

In alkaline media, the electrocatalyst requires energy to break the H–O–H bonding before chemisorption and desorption of hydrogen intermediate (H_{ads}) to produce H₂, as illustrated in eqn (1)–(3).¹ The Volmer is the rate-determining step (RDS), which is initial H–O–H cleavage, followed by chemisorption of the H_{ads} onto active sites (M) of noble metal electrocatalyst, while the HER subsequently occur either by eqn (2) (Tafel) or (3) (Heyrovsky) depending on the nature of the electrocatalyst and values of Tafel slope for H₂ production, as the H_{ads} recombine to yield H₂ or the catalyst continuously cleave water molecule and desorbed the H_{ads} to produced H₂,

respectively. The latter (eqn (3)) may mostly be preferred for efficient HER electrocatalysis in alkaline conditions because of a limited amount of H_{ads} which could only be generated by splitting water.²



HER is extremely sluggish in alkaline compared to the acidic media due to the initial water dissociation, instability of adsorbed hydrogen (H_{ads}) and ultimately large overpotential,² hence explaining the preference of platinum (Pt)-based electrocatalysts for efficient catalysis of HER in alkaline electrolyte. According to density functional theory (DFT), the theoretical H₂

Molecular Sciences Institute, School of Chemistry, University of the Witwatersrand, Private Bag 3, PO Wits, Johannesburg 2050, South Africa. E-mail: Kenneth.ozoemena@wits.ac.za; Tel: +27 11 717 6730



binding energy (E_{ads}) of palladium (Pd(111), $E_{\text{ads}} = -0.48$ eV) is close to that of Pt (Pt(111), $E_{\text{ads}} = -0.43$ eV), with excellent HER activities.³ Moreover, Pd-based electrocatalysts have proved to exhibit improved electrocatalytic performance in alkaline conditions.⁴ Hence, Pd-based electrocatalysts are viable substitute electrocatalysts for HER in an alkaline medium because of their high selectivity for H_2 binding, rapid desorption of H_{ads} , quick water splitting and transformable formation of H_{ads} to produce highly purified H_2 gas.⁵

Presently, several attempts are being made to reduce the cost of HER by using low-Pd loaded electrocatalyst on various carbon supports including carbon fibre,⁶ carbon paper substrate,⁷ Vulcan XC-72,⁸ graphitic nanofiber,⁹ and reduced graphene oxide,¹⁰ to mention a few. Although reports on these carbon-based supports show good results, a lot still needs to be done to enhance the electrocatalytic performance in terms of current density, energetics and kinetics. To our knowledge, there are little reports on the use of metal-organic framework-derived carbons (MOFDC) for HER and OER in alkaline electrolyte.¹¹ The choice of Co-MOF sacrificial template to synthesize novel carbon support (MOFDC) is because of the interesting inherent properties of MOF such as tunable pore size, enhanced surface area, electron density, electrical conductivity and thermal stability, and the ease of Co removal after carbonization by etching with acid.^{12,13}

This work describes the first report on the effect of MOFDC as a support for Pd electrocatalyst for HER activities. It is clearly shown that MOFDC significantly enhances both the energetic and kinetics of HER when compared to its analogue and many literature reports using other carbon-based supports.

2. Experimental

Nanostructured palladium electrocatalyst supported on MOFDC (Pd/MOFDC) was synthesized using previously reported microwave-assisted synthesis (summarized in Fig. 1).¹⁴ In brief, cobalt nitrate hexahydrate ($\text{Co}(\text{NO}_3)_6 \cdot 6\text{H}_2\text{O}$, 0.4366 g), 4,4'-biphenyldicarboxylic acid (BPDC, 0.3634 g) and triethylamine (TEA, 1.5 mL) were mixed in a flask containing dimethylformamide (DMF, 50 mL) and stirred for 15 min to obtain a homogeneous mixture. The mixture was then heated in a microwave (600 W, 150 °C, 30 min) forming precipitates, which were washed and dried in vacuum (60 °C) to obtain solid cobalt-based metal-organic frameworks (Co-MOF). The Co-MOF was then annealed from room temperature to 600 °C at 5 °C min^{-1} and then to 800 °C and maintained for 5 h. The resulting solution formed was cobalt nanoparticles on metal-organic frameworks-derived carbon (Co/MOFDC). The Co/MOFDC was then chemically etched with hydrochloric acid (3.0 M, 10 mL) to remove the cobalt nanoparticles, resulting in MOFDC. Pd nanoparticles (20 wt%) were dispersed onto the MOFDC by following this procedure: potassium tetrachloropalladate crystals (K_2PdCl_4 , 61.35 mg) were dissolved in EG (50 mL) and stirred for 30 min and pH of the solution was raised to 12 using NaOH (1.0 M). Then, the MOFDC (80 mg) was added and further stirred for 30 min. The mixture was irradiated with MW (600 W, 140 °C, 1 h) to disperse Pd nanoparticles on the support, after which the pH of the resulting product (Pd/MOFDC) was lowered to 3, using nitric acid (HNO_3 , 0.1 M). The final product was washed and dried (80 °C, 4 h) in a vacuum oven. A similar procedure was followed for making Pd/carbon black (CB).

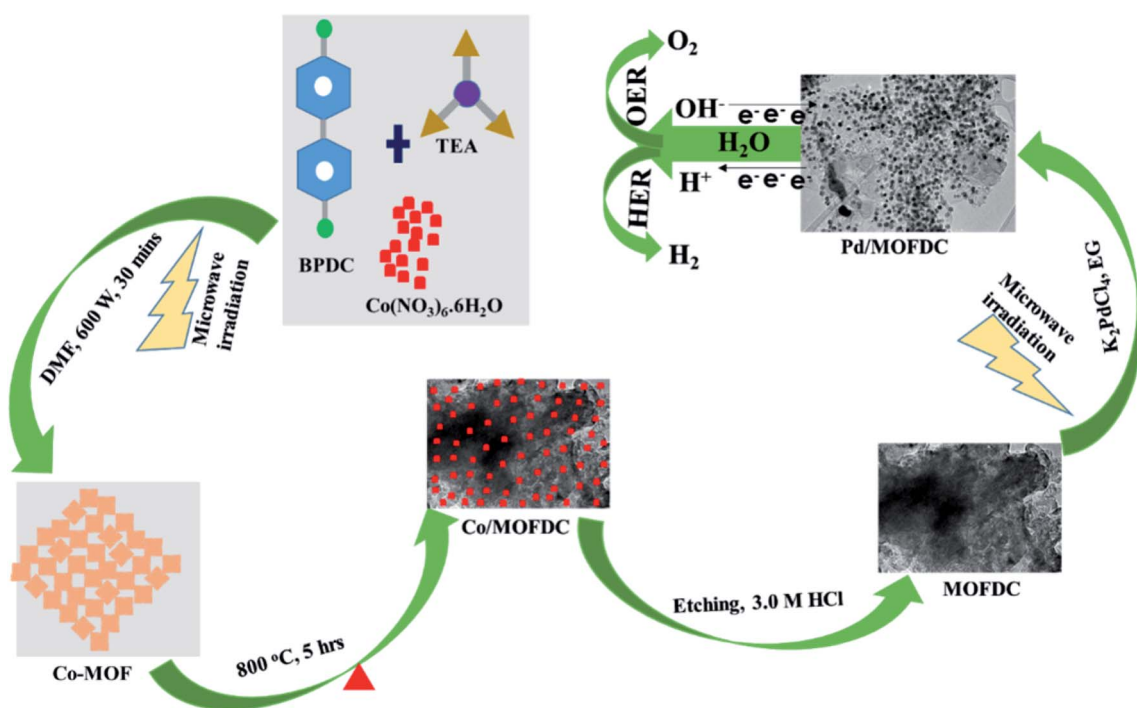


Fig. 1 Schematic illustration for the synthesis of Pd/MOFDC and Pd/CB electrocatalysts.



The physical properties of the materials and electrocatalysts were thoroughly probed using Raman spectroscopy (Horiba LabRam HR Raman spectrometer equipped with Olympus BX41 microscope), powdered X-ray diffraction (Bruker D2 XRD), transmission electron microscope (FEI Tecnai T12 Sprint TEM), Brunauer–Emmett–Teller (BET, Micrometric Tristar 3000) and thermal gravimetric analysis (PerkinElmer TGA 4000). All electrochemical measurements were carried out using a rotating disk electrode (RDE) with AUTO LAB PGSTAT204. The HER kinetics on the Pd/MOFDC and Pd/CB were investigated utilizing a conventional three-electrode system: the working electrode is a glassy carbon electrode (GCE, 5 mm diameter) modified with the Pd/MOFDC (GCE-Pd/MOFDC) and Pd/CB (GCE-Pd/CB) while platinum wire and Ag|AgCl, 3.0 M KCl were employed as counter and reference electrodes, respectively. Before the measurements, electrocatalyst inks were prepared and modified on the GCE as follow: 2 mg of each electrocatalyst powder was dispersed in a mixture of ethanol (2 mL) and Nafion (5 wt%, 50 μ L) and ultrasonically mixed for uniform distribution. Each electrocatalyst ink (20 μ L) was coated on the polished surface of the GCE and allowed to dry in the air to afford Pd catalyst loading ($0.0199 \text{ mg cm}^{-2}$). The HER experiment was carried out in freshly prepared KOH electrolyte

(0.1 M) at a controlled and varied temperature in water-bath thermostat. Moreover, electrochemical impedance spectroscopy (EIS) was used to confirm the HER kinetics at room temperature, 1600 rpm, overpotential 0.2 V vs. RHE and frequency range (100 kHz to 0.1 Hz). All potentials are referred to reversible hydrogen electrode (RHE) with conversion formula: $\text{RHE} = E_{\text{Ag|AgCl}} + 0.197 + 0.059 \text{ pH}$, where $\text{pH} = 12.57$.

3. Results and discussion

3.1 Physical characterization: Raman, XRD, BET and TEM measurements

The chemical bond vibrations of the Co-MOF, Co/MOFDC, MOFDC and Pd/MOFDC were studied using Raman spectroscopy (Fig. 2a). The spectra show the Co–O linkage and the organic frameworks confirmed the synthesis of the Co-MOF,¹⁴ which was broken down after carbonization at high temperature, confirmed with TGA (Fig. 3), forming the Co/MOFDC with distinct vibrational modes of Co metal and D and G bands for the MOFDC. Chemically etched Co/MOFDC removed most of the Co nanoparticles, as only the D and G bands remain in the formation of MOFDC. Dispersion of Pd nanoparticles on the

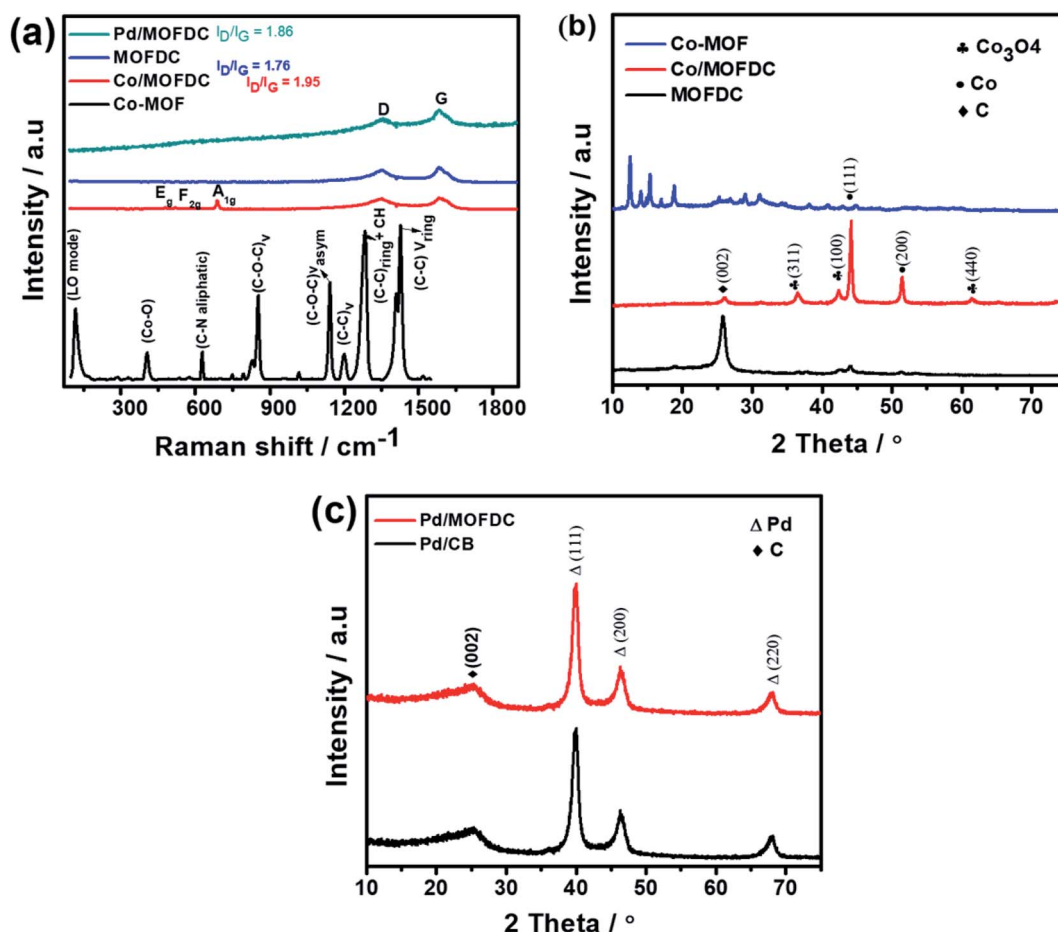


Fig. 2 (a) Raman spectral of Co-MOF, Co/MOFDC, MOFDC, and Pd/MOFDC, XRD of (b) Co-MOF, Co/MOFDC and MOFDC, and (c) Pd/MOFDC and Pd/CB.

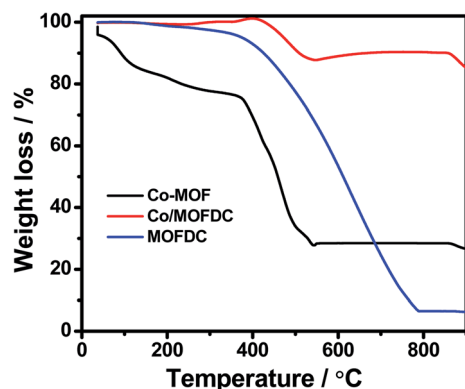


Fig. 3 TGA profiles under air condition of Co-MOF, Co/MOFDC and MOFDC.

MOFDC shifted slightly the position of D and G bands and raised the I_D/I_G value, showing increased defects.

Fig. 2b shows the XRD patterns of the Co-MOF, calcined product (Co/MOFDC) and derived carbon (MOFDC) obtained after chemical etching. The XRD pattern of the Co-MOF displays a well-crystalline material, which is fairly like the Co-MOF synthesized using benzene-1,3,5-tricarboxylic acid linkage.¹⁵ The slight difference in the crystallinity is ascribed to the difference in the architectural structure of chelating agents. After pyrolysis, the original peaks are replaced by series of peaks at 25.8° for hexagonal graphitic carbon (002), while the peaks at 36.5° , 42.6° , 44.0° , 51.7° , and 61.6° are attributed to a mixture of Co and Co_3O_4 nanoparticles with miller indices Co_3O_4 (311), Co_3O_4 (100), Co (111), Co (200) and Co_3O_4 (440) respectively.¹⁶ The chemically etched Co/MOFDC confirm that most Co and Co_3O_4 nanoparticles had been removed, giving rise to a pronounced carbon peak at 25.8° for the MOFDC (002) with little trace of peaks of Co/ Co_3O_4 remaining. These results agree with the Raman spectral (Fig. 2a). The XRD patterns of the Pd/MOFDC and Pd/CB are described in Fig. 2c. As observed, the hexagonal carbon (002) at 25.6° remains for the Pd/MOFDC and Pd/CB. The electrocatalysts exhibit well-defined crystalline peaks for the face-centered cubic structure of Pd nanoparticles at around 40.0° , 46.5° , 68.0° for Pd(111), Pd(200) and Pd(220), respectively.^{17,18}

Fig. 3 illustrates the TGA of the Co-MOF, Co/MOFDC and MOFDC. The TGA profile of the as-synthesized Co-MOF in air

Table 1 Comparative BET parameters for the precursor and electrocatalyst materials

BET analysis	Materials		
	Co-MOF	MOFDC	Pd/MOFDC
Specific surface area/ $\text{m}^2 \text{g}^{-1}$	24.41	143.67	150.20
Pore volume/ $\text{cm}^3 \text{g}^{-1}$	0.055	0.104	0.085
Pore size/nm	15.74	3.98	4.18

displays two decomposition steps. The first step indicates weight loss from room temperature to 134°C , showing loss of water molecules from the pores of the Co-MOF because the Co-MOF has strong adsorption for water molecules.¹⁶ The second weight loss is observed from 372°C to 541°C , ascribable to the decomposition of the BPDC frameworks of the Co-MOF and formation of Co/MOFDC. These results are consistent with the previous report for Co-based MOF using 2,5-dihydroterephthalic acid (DHTP)¹⁶ and corroborate the Raman (Fig. 2a) and XRD (Fig. 2b) analysis for the decomposition of the Co-MOF frameworks at high temperature. The formation of Co nanoparticles in the second phase of the Co-MOF was confirmed from the TGA curve of the Co/MOFDC, where some of the metallic Co nanoparticles are oxidized between 400°C and 541°C to Co_3O_4 nanoparticles, as the analysis was done in the air, and Co residue (86.6 wt%) remains after 900°C . The TGA profile of the MOFDC shows stability to 420°C , where weight loss gradually begins to 800°C and Co metal residue (6.5 wt%) remains after 900°C . This observation is like the report obtained for carbon microsphere.¹⁹

Fig. 4 compares the TEM micrographs of the MOFDC and Pd/MOFDC. The morphology of the MOFDC with no traces of metal nanoparticles, as seen in Fig. 4a. Pd nanoparticles are revealed in Fig. 4b. The average particle size of Pd in the Pd/MOFDC is estimated to be 6.8 nm (Fig. 4c).

The specific surface area (S_{BET}) of the Pd/MOFDC, MOFDC and Co-MOF are determined using BET analysis, summarized in Table 1. The Co-MOF has the lowest surface area and pore volume, but the highest pore size. After carbonization and chemically etched, the surface area and pore volume increased for the MOFDC, but the pore size reduced. Deposition of Pd nanoparticles on the

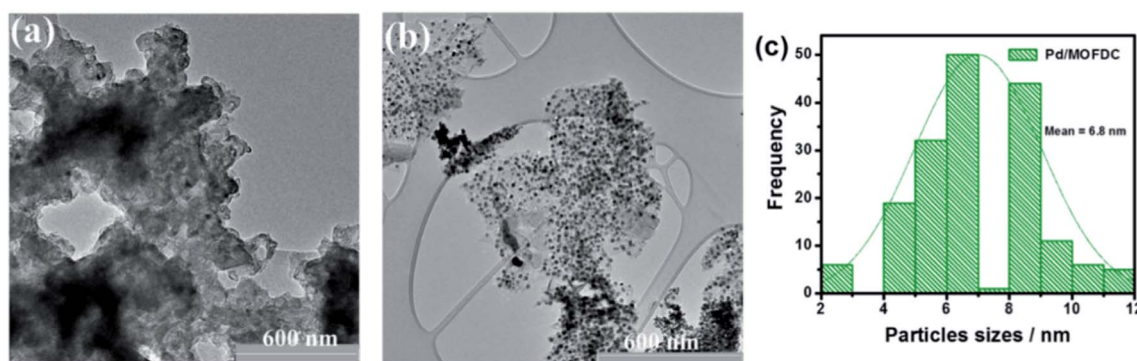


Fig. 4 TEM micrographs of (a) MOFDC, (b) Pd/MOFDC and, particles sizes distribution (c) Pd nanoparticles.



MOFDC increased slightly the surface area and pore size while the pore volume decreased. The increased surface area and pore size in the Pd/MOFDC may be traced to microwave irradiation during its synthesis, while the decreased pore volume is expected as Pd nanoparticles fill some of the pores.²⁰

3.2 Electrochemical measurements

3.2.1 Hydrogen evolution reaction (HER) study. Electrochemical activities of the Pd/MOFDC and Pd/CB electrocatalysts

toward HER were obtained using LSV at various rotation speeds (400, 900, 1600, 2500, 3600 and 4900 rpm) at a scan rate of 5 mV s⁻¹ in N₂-deaerated 0.1 M KOH electrolyte. Cathodic (HER) polarization curves of bare GCE and the electrocatalysts at 1600 rpm and other rotations for the electrocatalysts are illustrated in Fig. 5a and b, respectively. Current densities of the electrocatalysts increased for the HER in alkaline electrolyte, as the rotation speeds increased. The response of the Pd/MOFDC electrocatalyst is more than the Pd/CB at 1600 rpm (Fig. 5a)

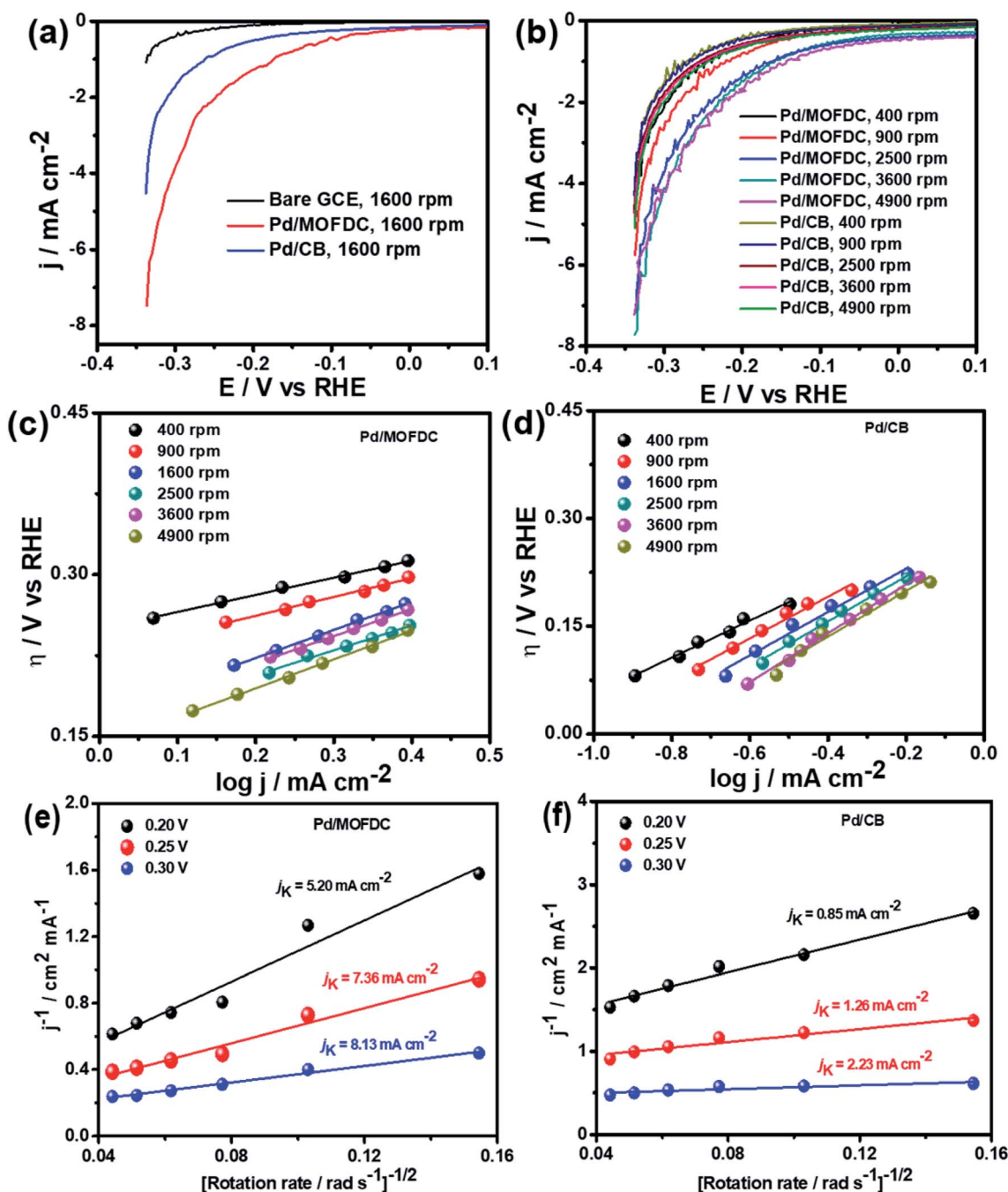


Fig. 5 (a) HER polarization curves of bare GCE and the electrocatalysts at 1600 rpm, (b) the electrocatalysts at different rotations, 5 mV s⁻¹ and 298 K, corresponding HER Tafel plots (c) Pd/MOFDC, (d) Pd/CB, and (e and f) Koutecky–Levich plots of the electrocatalysts in N₂-deaerated 0.1 M KOH solution.

and all other rotations (Fig. 5b). These observations could be traced to the modification of electron properties of the Pd by the increased defect of the MOFDC (Fig. 2a) and contributions from the Co metal residue TGA (Fig. 3). The electrochemical active surface area (ECSA) of the Pd/MOFDC and Pd/CB electrocatalysts was determined by running CV in KOH solution only, then PdO reduction for the catalysts was integrated, evaluated and are previously recorded as 263.4 cm² mg⁻¹ and 235.3 cm² mg⁻¹, respectively.¹⁴

To understand the HER kinetics, the polarization curves were modelled to the typical Tafel equation, as given in eqn (4) and (5).

$$j = -j_o e^{\left(\frac{-\alpha_c z F}{RT} \times \eta\right)} \quad (4)$$

Taking the log of eqn (4), re-arranging and making the overpotential (η/V vs. RHE) as the subject lead to the cathodic and anodic Tafel equations (eqn (5) and (6), respectively):

$$\text{Cathodic Tafel : } \eta = \frac{2.303RT}{\alpha_c z F} \log j_{o,s} - \frac{2.303RT}{\alpha_c z F} \log j_c \quad (5)$$

$$\text{Anodic Tafel : } \eta = \frac{2.303RT}{(1 - \alpha_a) z F} \log j_{o,s} - \frac{2.303RT}{(1 - \alpha_a) z F} \log j_a \quad (6)$$

where j_c and j_a represent the cathodic and anodic current densities (mA cm⁻²), respectively; $j_{o,s}$ is the exchange current density (mA cm⁻²), R is the universal gas constant, T is absolute temperature, F is Faraday constant, α_a and α_c are the anodic and cathodic electron transfer coefficients, z is the number of electrons involves in electrode reaction ($z = 1$). The Tafel plots of the electrocatalysts are presented in Fig. 5c and d. The kinetic parameters of the electrocatalysts for HER in N₂-deaerated 0.1 M KOH are summarized in Table 2.

The Pd/MOFDC electrocatalyst shows higher $j_{o,s}$ values at all the rotations speeds than the Pd/CB electrocatalyst and compared literature (see Table 3) because of ease of continuous H–O–H cleavages and more facile desorption of H_{ads} from the active sites (M) of Pd and increased rates of H₂ production, with agitation during HER as the rotation speed increased, as the M–H_{ads} bond is predominantly moderated by van der Waals forces.²¹ The H_{ads} present in this medium is continuously generated by electrocatalytically splitting water for H₂ production. Compared to most reports, the Pd/MOFDC also shows higher mass activity ($j_{o,m}$) of 58.63 mA mg⁻¹ at 1600 rpm in alkaline condition, due to the ease of continuous water splitting, yielding MH_{ads}, and subsequently desorption of the H_{ads} from the active sites of the Pd catalyst to eventually produce H₂.²²

Table 3 compares HER kinetics of the Pd/MOFDC with the Pd/CB and literature. The HER onset overpotential (onset η) values of 35 mV and 56.7 mV were obtained for the Pd/MOFDC and Pd/CB, with corresponding overpotential (η) values (at 2.5 mA cm⁻²) of 273.2 mV and 324.4 mV, respectively. The less η values of the Pd/MOFDC suggests lower energy is required for the evolution of hydrogen relative to other electrocatalysts, due to its ease of continuous water splitting for H₂ production. Tafel slope of the electrocatalysts for the HER is a parameter employed to explain that the catalysts continuously split water,

Table 2 Kinetic parameters of the electrocatalysts for HER in N₂-deaerated 0.1 M KOH solution at different rotation, 298 K and 5 mV s⁻¹

Kinetic parameters	Electrocatalysts	
	Pd/MOFDC	Pd/CB
@400 rpm		
$b_c/\text{mV dec}^{-1}$	159.3	258.0
$j_{o,s}/\text{mA cm}^{-2}$	0.1272	0.0614
α_c	0.37	0.23
@900 rpm		
$b_c/\text{mV dec}^{-1}$	175.1	290.1
$j_{o,s}/\text{mA cm}^{-2}$	0.1506	0.0875
α_c	0.34	0.20
@1600 rpm		
$b_c/\text{mV dec}^{-1}$	261.1	301.9
$j_{o,s}/\text{mA cm}^{-2}$	0.2226	0.1089
α_c	0.23	0.20
@2500 rpm		
$b_c/\text{mV dec}^{-1}$	231.5	314.5
$j_{o,s}/\text{mA cm}^{-2}$	0.2030	0.1264
α_c	0.26	0.19
@3600 rpm		
$b_c/\text{mV dec}^{-1}$	252.9	339.4
$j_{o,s}/\text{mA cm}^{-2}$	0.2185	0.1537
α_c	0.23	0.17
@4900 rpm		
$b_c/\text{mV dec}^{-1}$	266.3	318.7
$j_{o,s}/\text{mA cm}^{-2}$	0.2943	0.1495
α_c	0.22	0.19

even after the initial water splitting (Volmer). The high Tafel slopes of the catalysts suggest that Heyrovsky reaction (eqn (3)) proceeds immediately after the RDS (eqn (1)).²³ Thus, Volmer–Heyrovsky processes may predominate as the HER mechanism, as the process requires continuous H–O–H cleavage, adsorption of H (MH_{ads}) and desorption of the H_{ads}.²⁴ This assumption agrees with the study of free energy diagram of HER in alkaline conditions, which proved that Volmer–Heyrovsky mechanism dominate.²⁵ However, high Tafel slopes (160–266 mV dec⁻¹) obtained here than the theoretical values for Volmer and Heyrovsky processes, have previously been ascribed to high hydrogen adsorption onto the active sites of polycrystalline Pd electrocatalysts, as supplementary reaction step,^{26,27} and are also reported in the compared literature (see Table 3).

Koutecky–Levich plots of the electrocatalysts are employed to separate kinetic current from the mass transfer as the rotation speed increased, shown in Fig. 5e and f at varied overpotentials 0.20, 0.25 and 0.30 V (vs. RHE). The kinetic currents (j_k) were extrapolated from the intercept ($1/j_k$), as it is potential-dependent. At the overpotentials studied, the Pd/MOFDC records j_k values of 5.20, 7.36 and 8.13 mA cm⁻², while the Pd/CB records 0.85, 1.26 and 2.23 mA cm⁻², respectively. Then, heterogeneous rate constants (k^0) of the electrocatalysts were determined from the j_k values and averaged, following the



Table 3 Comparison of electrochemical HER activity of the electrocatalysts with literature in the alkaline electrolytes at 1600 rpm and 5 mV s^{-1} in terms of onset overpotential (onset η), Tafel slope (b_c), exchange current density ($j_{o,s}$) and mass activity ($j_{o,m}$)

Electrocatalysts	Electrolytes	Onset $\eta/\text{mV vs. RHE}$	$b_c/\text{mV dec}^{-1}$	$j_{o,s}/\text{mA cm}^{-2}$	$j_{o,m}/\text{mA mg}^{-1}$	Ref.
Pd/MOFDC	0.1 M KOH	35.2	261	0.2226	58.63	This work
Pd/CB	0.1 M KOH	56.7	302	0.1089	25.62	This work
Pd/C-500 °C	0.1 M KOH	60	148	0.1220	21.00	28
f-MWCNTs@Pd/TiO ₂	0.1 M KOH	<100	130	0.06	n/a	29
PdNiMo film	0.1 M KOH	85	227	n/a	n/a	22
rGO-Au ₄₈ Pd ₅₂	0.1 M KOH	80	149	0.1300	50.00	30
Pd-CN _x	0.5 M KOH	~89	150	0.2450	16.00	31
Pd	1.0 M KOH	n/a	210	0.1259	n/a	32
NiCo ₂ P ₄	1.0 M KOH	~98	34.3	0.45	n/a	33
Pd-FeO _x (OH ₂) _{2-2x}	0.1 M KOH	50	135	0.17	n/a	34

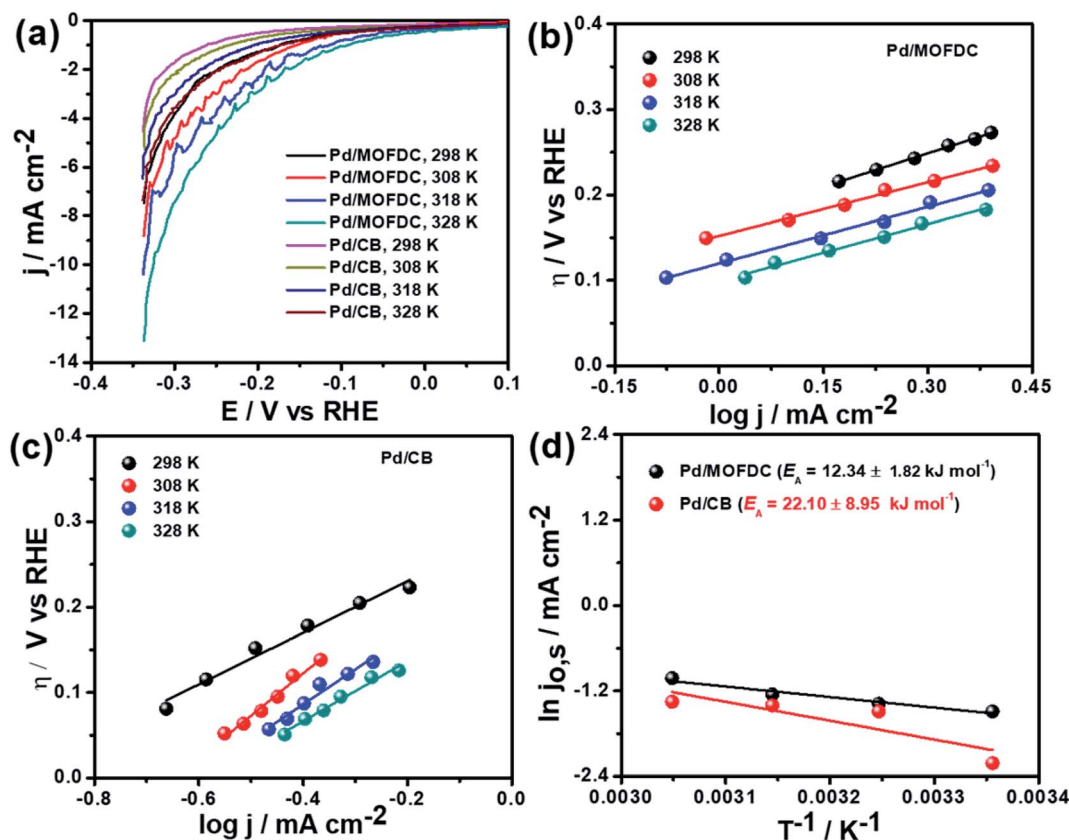


Fig. 6 (a) HER polarization curves of the electrocatalysts at 1600 rpm, 5 mV s^{-1} and different temperatures, corresponding HER Tafel plots of (b) Pd/MOFDC, (c) Pd/CB and (d) Arrhenius plots of the electrocatalysts in N_2 -deaerated 0.1 M KOH solution.

relationship ($j_k = nFk^0C$). Hence, mean k^0 values of 3.57×10^{-4} and $7.53 \times 10^{-5} \text{ cm s}^{-1}$ were calculated for the Pd/MOFDC and Pd/CB, respectively. These results show relatively facile HER activity concerning high j_k and k^0 values are also observed for the Pd/MOFDC, whereas the Pd/CB displays more sluggish HER kinetic. The same observation was recorded for the mass transfer with increased $j_{o,s}$ and $j_{o,m}$ values obtained for the Pd/MOFDC at all rotation speeds.

Temperature-dependence HER activities on the electrocatalysts in N_2 -deaerated 0.1 M KOH solution at 1600 rpm and

5 mV s^{-1} were studied at four different temperatures (298, 308, 318 and 328 K). The HER polarization curves of the Pd/MOFDC and Pd/CB electrocatalysts are displayed in Fig. 6a. To understand the effect of temperature on the HER, the polarization curves were also modelled to the conventional Tafel plots (eqn (5)), as shown in Fig. 6b and c.

The kinetic parameters of the temperature-dependent HER in N_2 -deaerated 0.1 M KOH solution on the electrocatalysts, at 1600 rpm and 5 mV s^{-1} , are summarized in Table 4. The $j_{o,s}$ values for the HER increased with increasing temperature. At all



Table 4 Temperature-dependence kinetic parameters of HER in N₂-deaerated 0.1 M KOH solution on the electrocatalysts at 1600 rpm, 5 mV s⁻¹ and different temperatures

Kinetic parameters	Electrocatalysts	
	Pd/MOFDC	Pd/CB
@298 K		
$b_c/\text{mV dec}^{-1}$	261.1	301.9
$j_{o,s}/\text{mA cm}^{-2}$	0.2226	0.1089
α_c	0.23	0.20
@308 K		
$b_c/\text{mV dec}^{-1}$	205.1	496.5
$j_{o,s}/\text{mA cm}^{-2}$	0.2513	0.2255
α_c	0.30	0.12
@318 K		
$b_c/\text{mV dec}^{-1}$	220.9	409.8
$j_{o,s}/\text{mA cm}^{-2}$	0.2871	0.2455
α_c	0.29	0.15
@328 K		
$b_c/\text{mV dec}^{-1}$	222.9	353.5
$j_{o,s}/\text{mA cm}^{-2}$	0.3597	0.2585
α_c	0.29	0.27

the temperatures studied in this work, the Pd/MOFDC electrocatalyst showed extremely higher $j_{o,s}$, relative to the Pd/CB and literature. This observation could be due to the incremental ease of continuous splitting of water on the Pd/MOFDC electrocatalyst as the temperature increases for H₂ production. This hypothesis agrees with the previous report that H–O–H splitting is enhanced at elevated temperatures.^{35,36}

Arrhenius equation was further employed to determine the minimum amount of energy required (activation energy (E_A)) for the electrocatalysis of HER to occur. Fig. 6d indicates the Arrhenius plots (plot of the natural logarithm of exchange current ($\ln j_{o,s}$) against the reciprocal of temperature (T^{-1})) where the E_A was extrapolated from the slope ($\frac{-E_A}{R}$) and calculated as $12.34 \pm 1.82 \text{ kJ mol}^{-1}$ and $22.10 \pm 8.95 \text{ kJ mol}^{-1}$ for the Pd/MOFDC and Pd/CB, respectively. The values of the E_A for these Pd-based catalysts were less than those previously reported for Pt/C ($\approx 18 \text{ kJ mol}^{-1}$).³⁷ The small value of the E_A for the Pd/MOFDC indicates reduced energy is required for continuous water splitting, perhaps due to lowered hydride phase formation for rapid production of H₂,³⁷ which is consistent with its onset overpotential and overpotential at 2.5 mA cm⁻². These observations are expected as Density Functional Theory (DFT) previously proved that the binding energy of hydrogen onto Pd-based catalyst is lowered with carbon supports that have increased electrons density.^{38,39}

Further investigation of the electrocatalysts for HER kinetics at room temperature, 1600 rpm and overpotential of 0.2 V vs. RHE was done using the EIS studies. The Nyquist plots (Fig. 7) with the modelled electrochemical equivalent circuit (inset) employed for fitting, revealed the HER kinetic of the electrocatalysts (listed in Table 5) during this process. The most

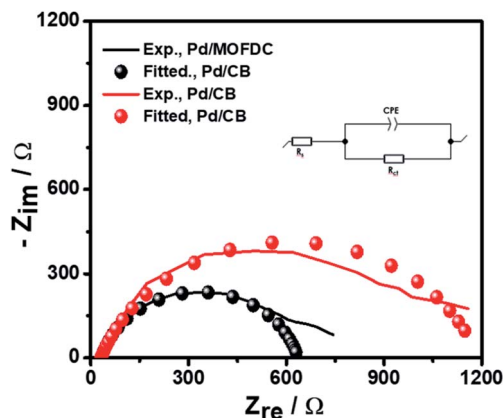


Fig. 7 EIS studies of the electrocatalysts for HER at overpotential 0.2 V, 1600 rpm, 5 mV s⁻¹ and 298 K.

Table 5 EIS kinetic data of the electrocatalysts for HER at overpotential 0.2 V vs. RHE, 1600 rpm, 5 mV s⁻¹ and 298 K

EIS parameters	Electrocatalysts	
	Pd/MOFDC	Pd/CB
R_s/Ω	32.64 ± 0.27	31.30 ± 0.26
R_{ct}/Ω	603.20 ± 0.59	1160.00 ± 0.32
$CPE/\mu\text{F s}^{(1-a)}$	79.93 ± 0.83	117.00 ± 0.49
a	0.84	0.79
$\chi^2/ Z $	1.68	1.66
$j_{o,s}/\text{mA cm}^{-2}$	0.2172	0.1129

important parameter is the charge transfer resistance (R_{ct}), which is used to determine the $j_{o,s}$, following eqn (7) below.

$$j_{o,s} = \frac{RT}{nFAR_{ct}} \quad (7)$$

The R_{ct} values of 603.20 Ω and 1160.00 Ω , resulted in calculated $j_{o,s}$ values of 0.2172 and 0.1129 mA cm⁻² for the Pd/MOFDC and Pd/CB, respectively. These values are approximately close to the kinetic values obtained using the Tafel plots.

3.2.2 Oxygen evolution reaction (OER) study. Out of curiosity, we also checked the ability of the Pd/MOFDC and Pd/CB to perform the oxygen evolution reaction (OER). As shown in Fig. 8a, the OER polarization curves for the electrocatalysts were conducted at 1600 rpm, 5 mV s⁻¹ and room temperature. This polarization curve was modelled to Tafel plots (eqn (6)), as shown in Fig. 8b. The data show a satisfactory current densities (j) of 18.40 mA cm⁻² and 14.68 mA cm⁻² with onset η of ca. 1.29 V and 1.49 V vs. RHE, which are higher than thermoneutral potential of water (1.23 V vs. RHE) for easy water splitting,^{40,41} and lowered than previously reported onset η value for the OER in the same medium,⁴² while Tafel slopes (b_a) of $77.68 \pm 12.81 \text{ mV dec}^{-1}$ and $112.30 \pm 4.96 \text{ mV dec}^{-1}$ for the Pd/MOFDC and Pd/CB, respectively, as the large differences of these values, could be traced to the Co metal residue. The low Tafel slope of the Pd/MOFDC is associated with better OER activity than Pd/



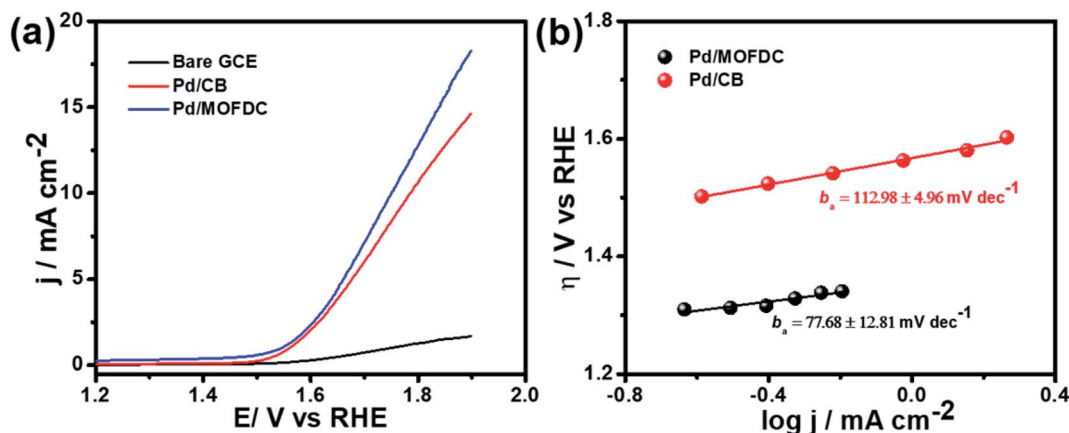


Fig. 8 (a) OER polarization curves and (b) OER Tafel plots of the electrocatalysts in N₂-deaerated 0.1 M KOH at 1600 rpm, 5 mV s⁻¹ and 298 K.

CB.^{41,43} These results show that the Pd/MOFDC electrocatalyst is not only good for HER but also excellent for OER, explaining its bi-functional behaviour for water electrolysis.

4. Conclusions

This work describes the first study of the use of MOFDC as efficient support for Pd electrocatalyst for HER and OER. The study reveals that the HER and OER activities on the Pd/MOFDC electrocatalyst are greatly improved, with extremely higher current densities compared to Pd/CB and literature. The enhanced HER activity of the Pd/MOFDC is attributed to the electronic properties of the Pd being modified by the increased electron density of the MOFDC and Co metal residue, resulting in the ease of continuously splitting of water to yield MH_{ads} and subsequently desorption of the H_{ads} to produce H₂, evidenced from the increased mass transfer ($j_{o,s}$ and $j_{o,m}$) and kinetic (j_K and k^0) parameters and the energy required to achieve this is very low. This observation was corroborated with the less E_A value of the Pd/MOFDC ($12.34 \pm 1.82 \text{ kJ mol}^{-1}$) than the Pd/CB ($22.10 \pm 8.95 \text{ kJ mol}^{-1}$). Additionally, the Pd/MOFDC displays satisfactory OER activity than its analogue, with lower onset η and b_a , and higher current response. This new study provides an opportunity for further research to rationally design more MOFDCs using different ligands and transition metals for the efficient electrochemical water-splitting process.

Conflicts of interest

There are no conflicts to declare.

Acknowledgements

This work was supported by National Research Foundation (NRF, Grant No. 113638) and the University of the Witwatersrand (Wits). A. K. Ipadeola is grateful for the award of NRF African Renaissance Doctoral Scholarship by the Department of Science and Innovation National Research Foundation in partnership with The World Academy of Science (DSI-NRF-TWAS). All opinions expressed and conclusions reached in this work

are those of the authors and not necessarily of the NRF, DST-NRF-TWAS or Wits.

References

- 1 K. Zeng and D. Zhang, *Prog. Energy Combust. Sci.*, 2010, **36**, 307.
- 2 J. R. Varcoe, P. Atanassov, D. R. Dekel, A. M. Herring, M. A. Hickner, P. A. Kohl, A. R. Kucernak, W. E. Mustain, K. Nijmeijer, K. Scott, T. Xu and L. Zhuang, *Energy Environ. Sci.*, 2014, **7**, 3135.
- 3 I. A. Pasti, N. M. Gavrilov and S. V. Mentus, *Adv. Phys. Chem.*, 2011, **2011**, 41.
- 4 K. I. Ozoemena, *RSC Adv.*, 2016, **6**, 89523.
- 5 D. G. Narehood, S. Kishore, H. Goto, J. H. Adair, J. A. Nelson, H. R. Gutierrez and P. C. Eklund, *Int. J. Hydrogen Energy*, 2009, **34**, 952.
- 6 B. Pierozynski, T. Mikolajczyk, M. Turemko, E. Czerwosz and M. Kozlowski, *Int. J. Hydrogen Energy*, 2015, **40**, 1795.
- 7 Y. X. Huang, X. W. Liu, X. F. Sun, G. P. Sheng, Y. Y. Zhang, G. M. Yan, S. G. Wang, A. W. Xu and H. Q. Yu, *Int. J. Hydrogen Energy*, 2011, **36**, 2773.
- 8 S. A. Grigoriev, P. Millet and V. N. Fateev, *J. Power Sources*, 2008, **177**, 281.
- 9 S. A. Grigoriev, M. S. Mamat, K. A. Dzhus, G. S. Walker and P. Millet, *Int. J. Hydrogen Energy*, 2011, **36**, 4143.
- 10 J. Li, P. Zhou, F. Li, J. Ma, Y. Liu, X. Zhang, H. Huo, J. Jin and J. Ma, *J. Power Sources*, 2016, **302**, 343.
- 11 S. Bhattacharyya, C. Das and T. K. Maji, *RSC Adv.*, 2018, **8**, 26728.
- 12 S. Pandiaraj, H. B. Aiyappa, R. Banerjee and S. Kurungot, *Chem. Commun.*, 2015, **50**, 3363.
- 13 W. Chaikittisilp, K. Ariga and Y. Yamauchi, *J. Mater. Chem. A*, 2013, **1**, 14.
- 14 A. K. Ipadeola, R. Barik, S. C. Ray and K. I. Ozoemena, *Electrocatalysis*, 2019, **10**, 366.
- 15 L. W. Aguiar, C. T. Pereira-da-Silva, H. H. Carline-de-Lima, M. P. Moises and A. W. Rinaldi, *AIMS Mater. Sci.*, 2018, **5**, 467.



- 16 H. Li, L. Chi, C. Yang, L. Zhang, F. Yue and J. Wang, *J. Mater. Res.*, 2016, **31**, 3069.
- 17 S. T. Bliznakov, M. B. Vukmirovic, L. Yang and R. R. Adzic, *J. Electrochem. Soc.*, 2012, **159**, F501.
- 18 T. Arunagiri, T. D. Golden and O. Chyan, *Mater. Chem. Phys.*, 2005, **92**, 152.
- 19 S. D. Mhlanga, K. C. Mondal, N. Naidoo, N. Kunjuzwa, M. J. Witcomb and N. J. Coville, *S. Afr. J. Sci.*, 2009, **105**, 304.
- 20 T. Zhang, H. Jin, Y. Fang, J. Guan, S. Ma, Y. Pan, M. Zhang, H. Zhu, X. D. Liu and M. L. Du, *Mater. Chem. Phys.*, 2019, **225**, 433.
- 21 K. Balasubramanian, P. Y. Feng and M. Z. Liao, *J. Chem. Phys.*, 1988, **88**, 6955.
- 22 J. Tang, X. Zhao, Y. Zuo, P. Ju and Y. Tang, *Electrochim. Acta*, 2015, **174**, 1041.
- 23 J. Wei, M. Zhou, A. Long, Y. Xue, H. Liao, C. Wei and Z. J. Xu, *Nano-Micro Lett.*, 2018, **10**, 75.
- 24 S. John St, R. W. Atkinson, R. R. Unocic, T. A. Zawodzinski and A. B. Papandrew, *J. Phys. Chem. C*, 2015, **119**, 13481.
- 25 J. Hu, C. Zhang, L. Jiang, H. Lin, Y. An, D. Zhou, M. K. H. Leung and S. Yang, *Joule*, 2017, **1**, 383.
- 26 Y. Pluntke and I. A. Kibler, *Electrocatalysis*, 2011, **2**, 192.
- 27 A. Safavi, S. H. Kazemi and H. Kazemi, *Fuels*, 2014, **118**, 156.
- 28 J. Durst, A. Siebel, C. Simon, F. Hasche, J. Herranz and H. A. Gasteiger, *Energy Environ. Sci.*, 2014, **7**, 2255.
- 29 G. Valenti, A. Boni, M. Melchionna, M. Cargnello, L. Nasi, G. Bertoni, R. J. Gorte, M. Marcaccio, S. Rapino, M. Bonchio, P. Fornasiero, M. Prato and F. Paolucci, *Nat. Commun.*, 2016, **7**, 13549.
- 30 J. A. S. B. Cardoso, L. Amaral, Ö. Metin, D. S. P. Cardoso, M. Sevim, T. Sener, C. A. C. Sequeira and D. M. F. Santos, *Int. J. Hydrogen Energy*, 2017, **42**, 3916.
- 31 T. Bhowmik, M. K. Kundu and S. Barman, *ACS Catal.*, 2016, **6**, 1929.
- 32 W. Sheng, M. Myint, J. G. Chen and Y. Yan, *Energy Environ. Sci.*, 2013, **6**, 1509.
- 33 R. Zhang, X. Wang, S. Yu, T. Wen, X. Zhu, F. Yang, X. Sun, X. Wang and W. Hu, *Adv. Mater.*, 2017, **29**, 1605502.
- 34 H. Liao, C. Wei, J. Wang, A. Fisher, T. Sritharan, Z. Feng and Z. J. Xu, *Adv. Energy Mater.*, 2017, **7**, 1701129.
- 35 M. Chhetri, S. Sultan and C. N. R. Rao, *Proc. Natl. Acad. Sci. U. S. A.*, 2017, **114**, 8986.
- 36 R. Subbaraman, D. Tripkovic, D. Strmcnik, K. C. Chang, M. Uchimura, A. P. Paulikas, V. Stamenkovic and N. M. Markovic, *Science*, 2011, **334**, 1256.
- 37 J. Durst, C. Simon, F. Hasche and H. A. Gasteiger, *J. Electrochem. Soc.*, 2015, **162**, F190.
- 38 M. Johansson, E. Skulason, G. Nielsen, S. Murphy, R. M. Nielson and I. Chorkendorff, *Surf. Sci.*, 2010, **604**, 718.
- 39 K. S. Joya, M. A. Ehsan, N. U. A. Babar, M. Sohail and Z. H. Yamani, *J. Mater. Chem. A*, 2019, **7**, 9137.
- 40 Y. Cheng and S. P. Jiang, *Prog. Nat. Sci.: Mater. Int.*, 2015, **25**, 545.
- 41 S. Xiong, P. Li, Z. Jin, T. Gao, Y. Wang, Y. Guo and D. Xiao, *Electrochim. Acta*, 2016, **222**, 999.
- 42 X. Liu, J. Dong, B. You and Y. Sun, *RSC Adv.*, 2016, **6**, 73336.
- 43 Y. Shao, M. Zheng, M. Cai, L. He and C. Xu, *Electrochim. Acta*, 2017, **257**, 1.

